Chemistry and Materials

The Center for Science Innovation

Research Article

Chem. Mater. 5 (1) 2026, 47-56

Electrodeposition of CZTS Thin Films with Na_2SO_3 Additive for Improved Photoelectrochemical Water Splitting Efficiency

Dyah Ayu Larasati*, Dyra Aulia Zhafirah, Reinardo Ramawijaya Widakusuma

Department of Chemistry, Faculty of Mathematics and Natural Science, Universitas Negeri Jakarta, Jl. Rawamangun Muka, Jakarta 13220, Indonesia

* Corresponding author: dyahayularasati2004@gmail.com

Received
31 August 2025

Received in revised form
12 November 2025

Accepted
20 November 2025

Published online
30 December 2025

DOI
https://doi.org/10.56425/cma.v5i1.118

Abstract

The global transition toward sustainable energy has accelerated research into clean hydrogen production, with photoelectrochemical (PEC) water splitting emerging as a promising pathway. In this study, Cu_2ZnSnS_4 (CZTS) thin films were prepared through one-step electrodeposition using sodium sulfite (Na_2SO_3) as an additive on indium tin oxide (ITO)-coated glass substrates. Structural characterization confirmed the formation of a crystalline kesterite phase, with the enhanced intensity of the (112) peak indicating improved crystallinity upon additive incorporation. Surface morphology and composition analysis revealed compact films with a uniform elemental distribution. PEC measurements showed a significant increase in photocurrent density from 7.4 mA/cm² to 22.3 mA/cm² at 1.47 V vs. RHE with Na_2SO_3 attributed to enhanced light absorption and efficient charge carrier separation. Optical analysis indicated a bandgap widening from 1.50 eV to 1.60 eV, consistent with a reduction in crystallite size. Impedance analysis showed lower charge transfer resistance under illumination. Hydrogen and oxygen evolution reaction (HER and OER) tests demonstrated lower overpotential and Tafel slopes, indicating faster reaction kinetics. Improved stability was confirmed by a positive shift in the corrosion potential (E_{corr}) and a lower corrosion current density (i_{corr}).. Overall, the addition of Na_2SO_3 enhanced the structural, optical, catalytic, and stability properties, making CZTS suitable for solar-driven hydrogen evolution.

Keywords: electrodeposition, CZTS, photoelectrochemical, additive

1. Introduction

The global energy crisis has become a major obstacle to economic growth and world peace, generating widespread international concern. Conventional fossil fuels not only are finite but also a significant source of environmental pollution [1]. Thus, alternative energies sources that are secure, clean, and globally available are in urgent demand. One promising solution is the storage of energy in the form of chemical fuels such as hydrogen. Hydrogen is a clean and efficient energy carrier due to its high mass-specific energy density, which enables on-demand energy generation [2].

However, for hydrogen to truly serve as a clean energy source, its production must also be clean, environmentally friendly, and economically competitive. A promising method, since its initial discovery by Fujishima and Honda in 1972, is photoelectrochemical (PEC) water splitting, which uses light energy to drive water electrolysis [3]. The PEC method uses photoelectrodes to produce hydrogen cleanly without generating toxic waste [4]. In this system, semiconductors act as photocatalysts, absorbing visible light and generating electron-hole pairs, which then drive redox reactions in the electrolyte [5,6]. An external circuit further supports the system by facilitating the flow of electrons from the photoanode to the photocathode to enable efficient redox reactions [7].

A key advantage of the PEC method is the integration light absorption and the photocatalytic reaction in a single system, as opposed to the two-step process required in photovoltaic-electrolyzer (PV-EC) systems [8]. PEC systems are also less dependent on critical raw materials (CRMs),

can utilize thermal radiation to enhance the reaction kinetics, and are more adaptable to day-night cycling [9].

Despite these advantages, PEC systems face several challenges, including a lack of long-term stability due to photocorrosion of certain photocatalysts and technical problems arising from the complexity of fabrication procedures [9]. Therefore, to achieve improved PEC performance, it is essential to develop semiconductor materials that are not only stable and efficient but also earth-abundant and low-cost [10]. One current strategy involves the fabrication of thin-film semiconductor materials for efficient charge separation and the acceleration of redox reactions [11]. The PEC system performance is greatly influenced by the light-harvesting properties of the photoelectrode. Materials with a high surface area and abundant active sites are required to facilitate interaction between the electrode surface and water molecules [12].

Among various quaternary semiconductor compounds, Cu_2ZnSnS_4 (CZTS) has recently attracted significant attention for use in thin-film solar cells due to several favorable properties, including p-type conductivity, a direct bandgap of approximately 1.5 eV, and a high absorption coefficient greater than 10^4 cm^{-1} in the visible spectrum [13]. As a member of the I_2-II-IV-VI_4 semiconductor family, CZTS shares structural and electronic similarities with $CuIn_xGa_{1-x}Se_2$ (CIGS), one of the most efficient materials currently utilized in solar cell technology. CZTS offers advantages over CIGS, including more abundant and less expensive constituent elements and a non-toxic composition [14].

However, CZTS suffers from drawbacks such as low charge transport rates, poor catalytic activity, and limited material stability, which collectively reduce its hydrogen evolution efficiency in PEC systems [15]. The use of additives offers a potential solution to these issues. They can function as brighteners and levelling agents that reduce surface roughness by promoting polarization during the electrodeposition process [16]. Additionally, additives may form complexes with metal ions and modulate reduction reactions [17]. One commonly used additive in electrodeposition is sodium sulfite (Na_2SO_3). According to a study by Xu et al [18], an electrolyte containing sulfite ions (SO_3^{2-}) can produce deposits that are high-quality, bright, and shiny, and form more stable complexes. Moreover, the presence of a small amount of sulfite in the solution can shift the disproportionation reaction to the left, thereby stabilizing the solution [19].

Therefore, in this study, CZTS thin films were fabricated by incorporating a Na_2SO_3 additive through an electrodeposition method as a strategy for enhancing the photoelectrochemical (PEC) water-splitting performance. This study was supported by characterizations using XRD, SEM, XRF, UV-Vis for bandgap determination, EIS, and tests for the hydrogen evolution reaction (HER) and oxygen evolution reaction (OER) to elucidate the material properties and the resulting PEC activity.

2. Materials and Method

2.1. Materials

All chemicals were of analytical grade and used as received without further purification. The following reagents, including copper(II) sulfate pentahydrate ($CuSO_4.5H_2O$), zinc sulfate heptahydrate ($ZnSO_4.7H_2O$), tin(II) chloride dihydrate ($SnCl_2.2H_2O$), thiourea ($SC(NH_2)_2$), trisodium citrate dihydrate ($Na_3C_6H_5O_7.2H_2O$), sodium sulfite (Na_2SO_3), hydrochloric acid (HCl), and potassium hydroxide (KOH), were purchased from Merck Indonesia. Ethanol 96% and distilled water were used in all experiments as well as cleaning solvents.

2.2. Synthesis of Cu-Zn-Sn-S (CZTS) alloy

The CZTS thin films were fabricated using a one-step three-electrode system electrodeposition technique from an aqueous electrolyte solution. In this setup, an Ag/AgCl (3 M KCl) electrode served as the reference, a platinum wire was used as the counter electrode, and an ITO-coated glass substrate functioned as the working electrode. The electrolyte contained 0.02 M $CuSO_4.5H_2O$, 0.02 M $ZnSO_4.7H_2O$, 0.02 M $SnCl_2.2H_2O$, 0.02 M $SC(NH_2)_2$, 0.001 M Na_2SO_3 as an additive, and 0.02 M $Na_3C_6H_5O_7.2H_2O$ as a complexing agent. The pH of the precursor solution was adjusted to 4-6 using 37% HCl. The Cu-Zn-Sn-S precursors were added progressively with 5-minute intervals and the solution was stirred for 30 minutes to ensure homogeneity. Before deposition, the ITO substrates were cleaned by sequential ultrasonication in ethanol and distilled water, followed by air-drying. The electrodeposition was performed potentiostatically at 30°C with an applied potential of -1.2 V vs. Ag/AgCl for 30 minutes [20].

2.3. Characterization

The elemental composition was determined by X-ray fluorescence (XRF). The surface morphology and topography were analyzed using a scanning electron microscope (SEM). The crystal structure and phase identification were examined by X-ray diffraction (XRD) on a Panalytical AERIS diffractometer.

2.4. Photoelectrochemical analysis

The photoelectrochemical properties of the CZT thin films were investigated using a Corrtest C310 workstation. A standard three-electrode quartz cell was used, with the CZT film as the working electrode, a platinum wire as the

counter electrode, and an Ag/AgCl (3 M KCl) electrode as the reference.

Photoelectrochemical (PEC) measurements were conducted using a solar simulator with a halogen lamp, calibrated to 1.5 G AM. Photocurrent responses were measured via linear sweep voltammetry (LSV) from −1.0 V to 1.5 V vs. Ag/AgCl at a scan rate of 50 mV/s in a 0.5 M Na_2SO_4 electrolyte. Electrochemical impedance spectroscopy (EIS) was performed under light irradiation in a frequency range from 100 kHz to 0.01 Hz with a 5 mV perturbation amplitude. The catalytic activity for the hydrogen evolution reaction (HER) and oxygen evolution reaction (OER) was evaluated in a 0.5 M KOH solution. LSV for HER was performed from −1.0 V to −2.0 V vs. Ag/AgCl, and for OER from 0.3 V to 1.5 V vs. Ag/AgCl, both at a scan rate of 50 mV/s.

All recorded potentials were converted to the reversible hydrogen electrode (RHE) scale using the following conversions:

$$E_{RHE} = E_{Ag/AgCl} + 0.6106 \text{ V (for 0.5 M } Na_2SO_4) \quad (1)$$

$$E_{RHE} = E_{Ag/AgCl} + 1.0059 \text{ V (for 0.5 M KOH)} \quad (2)$$

3. Results and Discussion

3.1. Morphology, composition, and structure analysis

Figure 1 shows the XRD patterns of the samples, which reveal the presence of multiple phases, in accordance with previous findings [21]. Distinct diffraction peaks for Cu-Zn-Sn-S (CZTS) were observed at 2θ angles of 34.5°, 39.8°, 40.6°, 50.0°, 58.2°, 62.4°, 65.2°, 70.6°, and 76.7°, corresponding to the (112), (200), (004), (114), (204), (301), (310), (215), and (231) crystal planes, respectively. Among these, the peaks at 34.5°, 39.8°, 50.0°, 58.2°, 70.6°, and 76.7° were indexed and confirmed to match the reflection planes of the kesterite CZTS structure (JCPDS No. 026-0575). The strongest peak, (112), indicates a preferred orientation, as it is the most intense peak in all CZTS thin film samples [22]. Additional XRD analysis of the complete device structure verified the phase purity and crystallinity, showing contributions from CdS (JCPDS No. 41-1049), ITO (JCPDS No. 89-4597), CZTS, and ZnO (JCPDS No. 36-1451), as reported by Peksu and Karaagac [22]. A significant enhancement in the intensity of the (112) peak in the CZTS thin films was observed, indicating improved crystallinity. This enhancement can be attributed to stress relief within the film, high lattice-matching, and increased surface contact area. The observed peaks were also consistent with ICDD card No. 03-065-0298, suggesting the formation of a cubic crystal structure with prominent diffraction along the (112) and (200) planes. Furthermore, a broad and relatively low-intensity peak corresponding to the (103) plane was observed in samples prepared with additives, suggesting partial crystallinity or structural disorder [22].

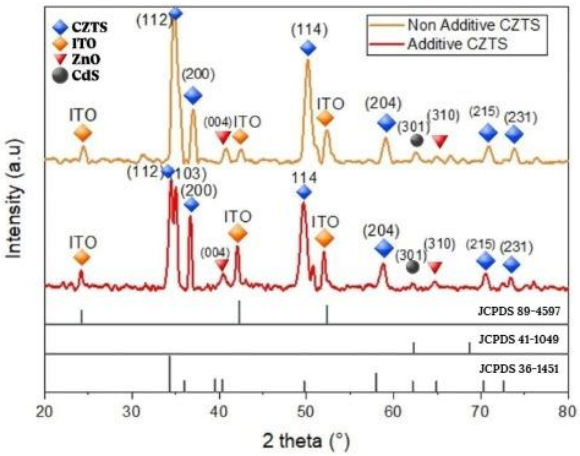

Figure 1. XRD pattern of CZTS thin films synthesized with additive and non-additive.

The sharpness and high intensity of the peaks reflect a high degree of crystallinity in the synthesized CZTS films [23]. The addition of Na_2SO_3 during electrodeposition reduced the average crystallite size from 7.1 nm (without additive) to 5.6 nm (with additive), as indicated by the peak broadening in the XRD patterns (calculated using the Scherrer equation). The decreased crystallite size enhances the surface area and the number of active sites, promoting the improvement of photocurrent generation and reduction of charge transfer [24]. To overcome sulfur deficiency during synthesis, two strategies were identified. The first involved the thermal oxidation of Na_2S, leading to the formation of sodium sulfite (Na_2SO_3) upon annealing, as reported [25]. The second strategy involved the direct addition of Na_2SO_3, which minimizes the oxidation of lattice S^{2-} ions. This, in turn, enhances the structural integrity and photoelectrochemical stability of the CZTS absorber layer [26].

Figure 2 shows top-view SEM images of the CZTS thin films. For both non-additive and additive samples, the film surfaces exhibit cracks and grain agglomeration. Such cracks are caused by internal stress that develops during and after deposition, due to factors such as differential shrinkage rates upon drying and cooling, as well as thermal expansion mismatches between film and substrate. This stress may be exacerbated at defect sites such as grain boundaries or surface defects, which act as stress concentrators that induce cracking [27].

In the non-additive sample, needle-like features measuring up to 20 µm are also observed. These features likely result from uncontrolled secondary crystal growth [28], indicating an imbalance between the nucleation and grain growth stages during film formation. The morphology of the non-additive CZTS film is also less

uniform, with spherical granular grains of varying sizes and a relatively high degree of agglomeration, resulting in a comparatively rough surface. The average grain size of this sample, determined via the linear intercept method, was 432 nm. This value is larger than the crystallite size obtained from XRD, indicating the agglomeration of CZTS crystallites [29].

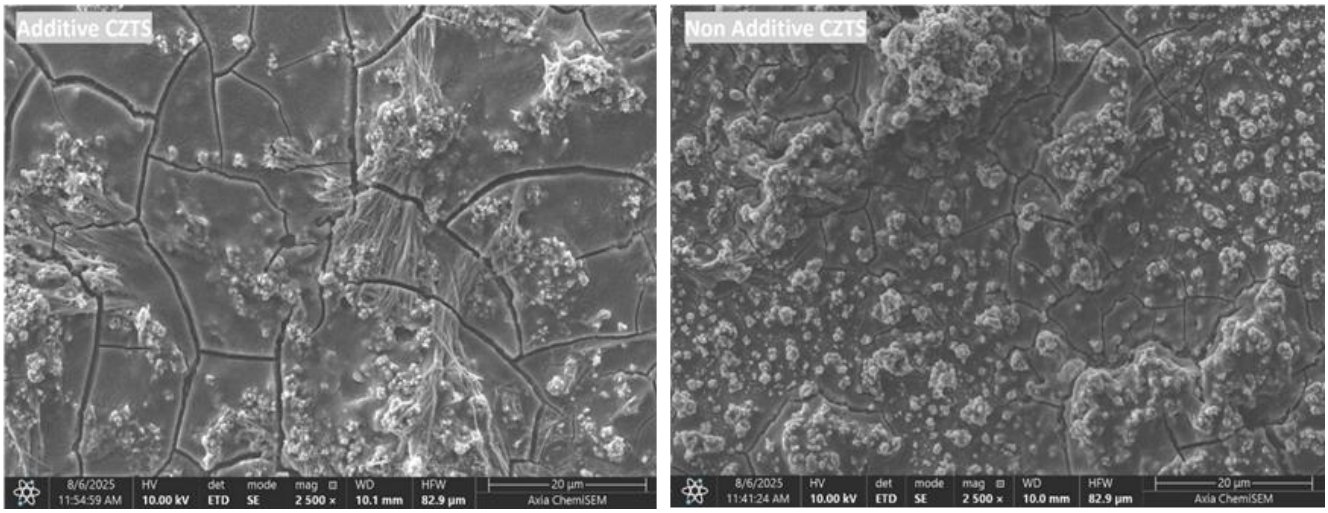

Figure 2. SEM images of CZTS alloys synthesized with additive and non additive.

In contrast, in the sample cast that was added with Na_2SO_3 as additive, although cracks and agglomeration were still present, particle distribution on the surface appeared more uniform with relatively homogenous grain sizes. Nearly the entire surface was a cover of spherical grains of relatively uniform size, without the needle shapes that were found in the non-additive sample. This sample had a mean grain size of 313 nm, which was smaller than that of the non-additive sample. This is attributed to the capacity of Na_2SO_3 in controlling the kinetics of crystal growth by adjusting the environment for electrodeposition [24].

To gain a better understanding of the accurate chemical composition and to ensure the homogeneity of the samples prepared, X-ray Fluorescence (XRF) spectroscopy was carried out. An overview of the chemical structure determined by XRF is tabulated in detail in Table 1. Corrected and normalized to account for the contribution of the Sn from the ITO substrate, X-ray fluorescence (XRF) results show that the addition of additives into the CZTS material significantly affects the elemental composition. A decrease in Cu content, an increase in Sn and S content, and a relatively consistent level of Zn were observed. In synthesis, the possible oxidation and rapid diffusion of Cu and Sn lead to non-uniform element distribution and incomplete reactions of CZTS formation[30]. This condition also aligns with Cu-poor CZTS characteristics, which has been found to promote high efficiency in solar cells, something that would imply the addition of additives improves CZTS performance compared to non-additive samples [31]. Further, the increase in sulfur concentration is also due to the contribution of Na_2SO_3 as a source of S^{2-} ions in the solution to facilitate the existence of sulfur bonds in the crystal structure of CZTS.

Table 1. Chemical compositions obtained from the XRF measurements of CZTS synthesized with additive and non-additive.

Element	CZTS (%)	CZTS-additive (%)
Cu	71.23	65.512
Zn	1.564	1.549
S	16.591	19.673
Sn	10.615	13.266

3.2. Photoelectrochemical analysis

The application of CZTS nanoparticle coatings onto the photoanode surface, particularly on ITO substrates, has been shown to significantly enhance photocurrent output by as much as two orders of magnitude. This improvement is attributed to the superior absorption capability in the visible light region and the effective separation of photogenerated electron-hole pairs, which together facilitate more efficient interfacial charge transport [32].

As illustrated in Fig 3, the photoelectrochemical (PEC) performance of CZTS films provides critical insight into the semiconductor's surface characteristics an important parameter for photovoltaic (PV) device optimization [33]. In particular, CZTS samples synthesized with the incorporation of Na_2SO_3 additive demonstrated a substantially enhanced photocurrent response, reaching 22.3 mA/cm² at an applied potential of 1.47 V vs. RHE. In contrast, samples synthesized without the additive exhibited a significantly lower photoresponse of only 7.4 mA/cm² at approximately 1.45 V. Linear sweep

voltammetry (LSV) was used to quantify photocurrent density across a potential window ranging from 0.4 V to 2.0 V vs. RHE [21].

Samples with added additives exhibit the highest overall energy conversion efficiency. The synthesis is performed under heating conditions, as at elevated temperatures, sulfur present in the atmosphere reacts with the CZTS precursors to form the desired CZTS phase [34]. The inclusion of Na_2SO_3 contributes to the stabilization of metallic species within the deposition environment, which supports the formation of uniform and stable CZTS films[26]. The photoelectrochemical characterization of sulfur-treated CZTS thin films confirms substantial improvements in power conversion efficiency, especially in the presence of Na_2SO_3 additives. This is further supported by optical studies (Fig 4), which reveal a slight increase in the bandgap energy of the CZTS films from 1.50 eV to 1.60 eV.

The small band gap increase is due to the fact that the additive improves the film quality and reduces defects/secondary phases, shifting the optical absorption edge to the higher energy. The observed widening of the bandgap is likely a consequence of reduced crystallite size induced by increased concentrations of the complexing agent during synthesis [24]. This bandgap tuning is critical, as it directly influences the solar energy conversion efficiency of the material. Under illumination, narrow band gap semiconductors like CZTS generate photogenerated electrons that are susceptible to recombination losses. The presence of a sacrificial reagent such as sulfite (SO_3^{2-}) in the electrolyte plays a vital role in suppressing undesirable back reactions by facilitating the reduction of S^{2-} to S^-, thereby maintaining sulfur availability throughout the synthesis process [32].

3.3. Electrochemical impedance spectroscopy analysis

Electrochemical impedance spectroscopy (EIS) measurements can be interpreted based on different frequency regions, each representing a specific resistance type. At low frequencies, the Warburg impedance appears, which corresponds to resistance related to mass transport limitations. The mid-frequency region reflects the charge transfer resistance at the electrode interface, while the high-frequency region is associated with the dielectric response of the solid-electrolyte interphase [32].

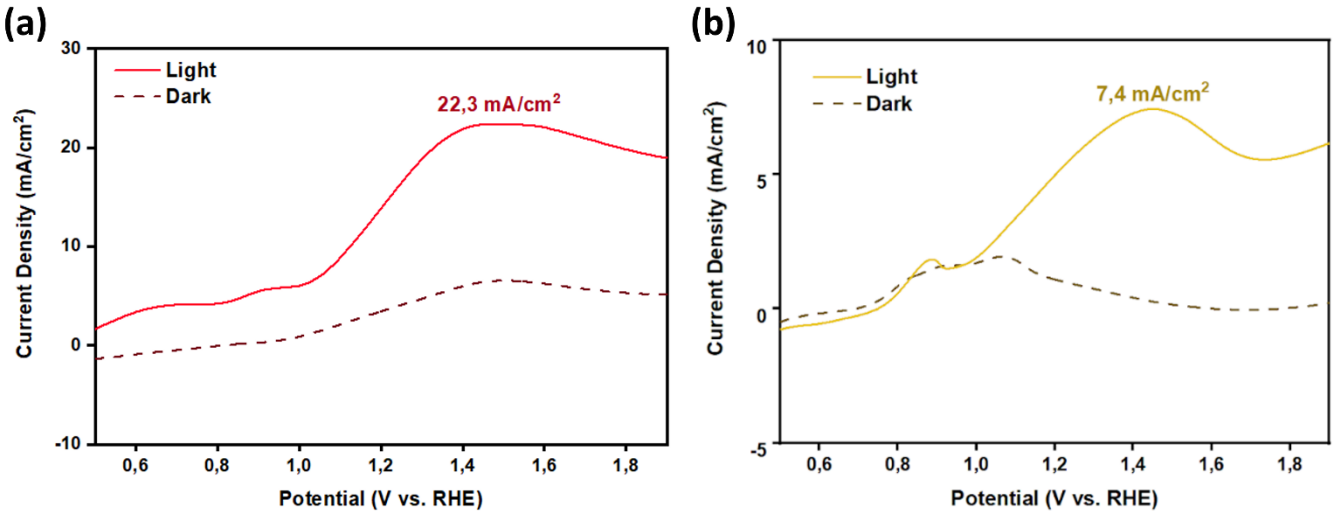

Figure 3. Photocurrent response under irradiation measured from CZTS synthesized (a) with additive (b) non additive, over a potential range of 0.4 V to 2 V vs RHE with scan rate at 50 mV/s in 0.5 M.

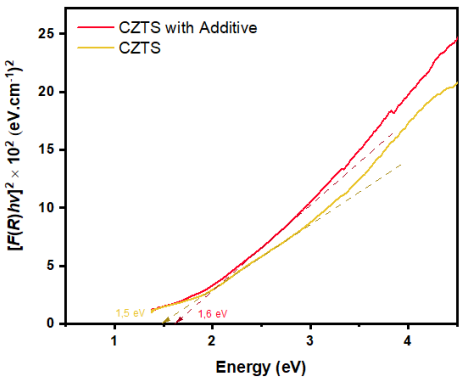

Figure 4. The bandgap values of CZTS synthesized A with additive and non-additive.

For all CZTS film-based photoanodes, EIS data were fitted using an equivalent circuit model that includes solution resistance (R_s), charge transfer resistance (R_{ct}), and capacitance (C_p). The equivalent circuit scheme used for simulation is displayed in the inset of Figure 5. The semicircular arc in the Nyquist plot is due to the charge transfer activity at the semiconductor/electrolyte junction

[24]. A smaller radius of the arc in the Nyquist diagram indicates a more efficient charge transfer process with reduced charge transfer resistance at the electrode–electrolyte interface [32]. In comparison to dark, the radius of the circular arc for both CZTS with and without additive under illumination is much smaller, indicating better separation of the photogenerated charge carriers and enhanced charge transfer efficiency[24]. In addition, under light exposure, the CZTS photoanodes exhibit a higher photocurrent density.

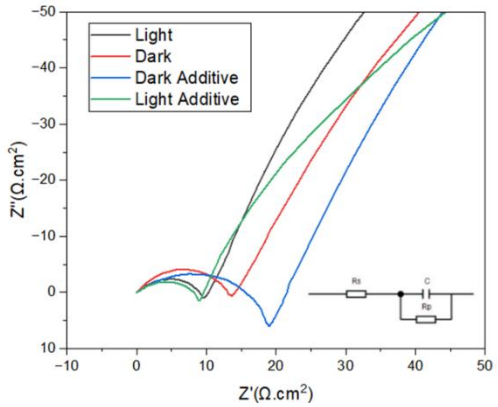

Figure. 5 Nyquist plots measured by simulated solar irradiation for CZTS synthesized with additive and non-additive.

This is because of the increased surface area-to-volume ratio of the material and more pronounced light absorption near the electrolyte interface [24]. The introduction of Na_2SO_3 as an additive during CZTS synthesis efficiently decreases the charge transfer resistance (Rct), particularly under illumination. It may be a consequence of improved homogeneity of the film surface, reduced defect density, and more effective electron transport due to photoexcitation [24].

Table 2. R_{ct} and R_s values of CZT*S* synthesized with additive and non-additive.

CZT	R_{ct}	R_s
Light non-additive	8.28 Ω	-6.64 Ω
Dark non-additive	12.38 Ω	23,01 Ω
Light additive	7.38 Ω	-6.28 Ω
Dark additive	16.01 Ω	38,47 Ω

3.4. HER and OER activities

The Linear Sweep Voltammetry (LSV) curves of the samples provide significant data on the catalytic activity of CZTS to accelerate the hydrogen evolution reaction (HER) and oxygen evolution reaction (OER) (Fig 6 A-B). In the case of HER, the Na_2SO_3-added CZTS sample exhibits lower overpotential of 10 mA/cm^2 compared to CZTS without additive. This indicates an incredible enhancement of HER catalytic activity because lower overpotential indicates a better reaction.

The HER process entails the transfer of two electrons from the electrode to protons, with an active catalyst required to reduce the energy barrier at each step of the reaction [17]. The reduction in overpotential with the introduction of Na_2SO_3 is due to the electron-donating nature of sulfite ions (SO_3^{2-}), with higher charge transfer at the electrode–electrolyte interface. This is a rise in the electron density on the electrode surface, and it becomes more reducing to reduce protons (H^+) into hydrogen gas (H_2). As a catalyst, CZTS provides active sites to adsorb and dissociate protons and to create H_2 [35]. When a voltage is applied, the protons in the electrolyte move to the negatively charged CZTS electrode and are attracted to available active sites. There, the protons receive electrons from the conductive nature of CZTS with and without the addition of an additive and undergo subsequent reaction to form hydrogen gas [21]. HER efficiency is also increased due to the suitable morphology of CZTS, providing more surface area and more active sites.

During OER, the overpotential for 10 mA current for the sample with CZTS added with Na_2SO_3 was found to be lower than the sample with CZTS without the addition of Na_2SO_3, indicating that the addition of Na_2SO_3 improves the activity of the catalyst towards oxygen evolution. The OER reaction proper involves the oxidation of water molecules to give oxygen gas (O_2), protons (H^+), and electrons (e^-), which occurs at the anode of an electrochemical cell. In this context, CZTS acts as an electrocatalyst that facilitates the transfer of electrons from water molecules to the conduction band of the material. CZTS can also form a protective oxide layer on its surface, such as CuO and SnO_2, resulting from the oxidation of the Cu_6Sn_5 phase, which contributes to improved charge transfer and resistance to corrosion [21]. The addition of Na_2SO_3 further enhances the performance of CZTS through the role of SO_3^{2-} as a reducing agent capable of removing passive oxide layers, thereby exposing more active sites for reaction, accelerating charge transfer, and supporting the overall efficiency of the OER.

The Tafel slope is an important parameter used to evaluate the reaction kinetics of an electrocatalyst. The Tafel slope value is obtained by plotting the logarithm of current density (j) against the overpotential (η), which has been corrected for solution resistance (iR-corrected), thereby reflecting how effectively the catalyst can convert overpotential into current. This parameter links the reaction rate to the magnitude of the overpotential, which refers to the additional voltage required beyond the

equilibrium potential for the reaction to proceed and produce products at the electrode surface [35].

In HER and OER reactions, CZTS sample with additives performed better compared to the sample without additives. For HER measurement, the Tafel slope of CZTS with additive was recorded at a lower 49 mV/dec, indicating faster hydrogen evolution and more effective reaction kinetics compared to 156 mV/dec for the sample without additive. Similarly, for the OER reaction, CZTS with additive showed a Tafel slope of 74 mV/dec, which is lower than the 104 mV/dec of the sample without additive.

A smaller Tafel slope indicates that less overpotential is required to achieve a specific current density, revealing a more efficient catalytic performance. The Tafel slope has been among the most significant analytical parameters and key indicators of reaction kinetics conventionally. Recent studies demonstrated that the Tafel slope is influenced by various intercorrelated aspects including catalyst composition, microstructural features, applied current density, and experimental conditions [36]. The accelerated activity in HER and OER is attributed directly to the presence of sulfite ions (SO_3^{2-}), which are electron donors that render the electrode surface more reductive to enable quicker hydrogen evolution, as well as reducing agents that strip the passive oxide layers on the surface, thereby enhancing OER efficiency.

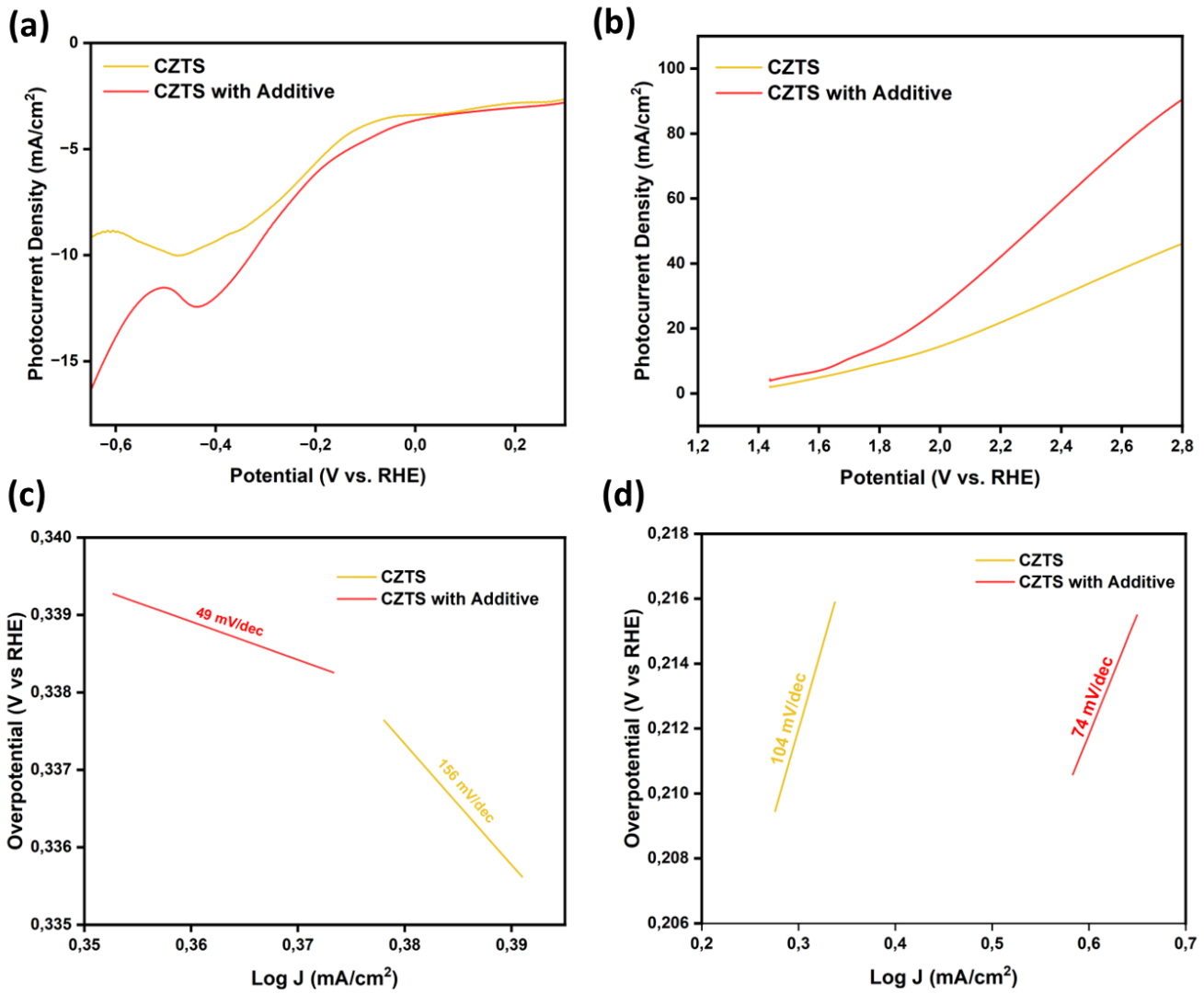

Figure 6. LSV curves of (a) HER and (b) OER of CZTS alloys testing. The OER and HER tests were conducted in 0.5 M KOH electrolyte with a scan rate of 50 mV/s. Tafel Slope of (c) HER and (d) OER of CZTS alloys under solar simulator irradiation.

Corrosion potential (E_{corr}) and corrosion current (i_{corr}) are important parameters to assess the stability of a catalyst for water splitting applications. E_{corr} is a thermodynamic descriptor representing the tendency of a metal to corrode in a specific environment. The more positive the E_{corr} value, the smaller the thermodynamic driving force for corrosion, the higher the corrosion resistance [37]. Meanwhile, a lower (more negative) i_{corr} value indicates a smaller corrosion rate [38]. Based on the results of Table 3, CZTS sample with additive possesses

superior corrosion resistance and stability, as demonstrated by more positive E_{corr} and more negative i_{corr} compared to the CZTS sample without additive, which displays more negative E_{corr} and larger i_{corr} value.

Table 3. The corrosion potentials (E_{corr}) and corrosion currents (i_{corr}) of CZTZ alloys synthesized *without additive* and *with additive*.

Sample	E_{corr} (V)	i_{corr} (mA)
CZTS	0,07	-1,16
CZTS with Additive	0,09	-1,24

4. Conclusion

This study demonstrates that the efficiency of photoelectrochemical (PEC) systems for water splitting can be significantly improved through the modification of Cu_2ZnSnS_4 (CZTS) material by adding sodium sulfite (Na_2SO_3) as an additive. This improvement is evidenced by a substantial increase in photocurrent density from 7.4 mA/cm² to 22.3 mA/cm², a reduction in overpotential and Tafel slope during the HER and OER processes, as well as a decrease in charge transfer resistance based on EIS results. Structural characterization also shows enhanced crystallinity, a more even morphology with good particle size distribution, and a widened bandgap, which support more efficient charge separation. Additionally, the material's stability improved, as indicated by a more positive E_{corr} value and a lower i_{corr} compared to the sample without the additive.

Author contributions

Dyah Ayu Larasati: Investigation, Formal analysis, Writing-original draft. **Dyra Aulia Zhafirah**: Investigation, Formal Analysis, Conceptualization. **Reinardo Ramawijaya Widakusuma:** Methodology, Software, Formal Analysis, Supervision.

Conflicts of interest

There are no conflicts to declare

Acknowledgement

The authors acknowledge that this work was funded by Universitas Negeri Jakarta.

References

[1] J. Ling, X. Zhang, T. Mao, L. Li, S. Wang, M. Cao, J. Zhang, H. Shi, J. Huang, Y. Shen, L. Wang, Electrodeposition of CdTe thin films for solar energy water splitting, *Materials*. **13** (2020). https://doi.org/10.3390/ma13071536.

[2] I. Gupta, R. Jain, A. Verma, Sheenam, Recent advances in copper kesterite thin film photocathodes for hydrogen production via water splitting: A review, *Materials Today: Proceedings*. (2024). https://doi.org/10.1016/J.MATPR.2024.05.042.

[3] A. FUJISHIMA, K. HONDA, Electrochemical Photolysis of Water at a Semiconductor Electrode, *Nature*. **238** (1972) 37–38. https://doi.org/10.1038/238037a0.

[4] F. Qureshi, M. Tahir, Photoelectrochemical water splitting with engineering aspects for hydrogen production: Recent advances, strategies and challenges, *International Journal of Hydrogen Energy*. **69** (2024) 760–776. https://doi.org/10.1016/J.IJHYDENE.2024.05.039.

[5] I. Ali, G. Imanova, T. Agayev, A. Aliyev, T.A. Kurniawan, A. Bin Jumah, Generation of hydrogen from various aqueous media using gamma radiation, *Journal of Radioanalytical and Nuclear Chemistry*. **333** (2024) 5161–5171. https://doi.org/10.1007/S10967-024-09670-9/METRICS.

[6] M. Nisar, N. Khan, M.I. Qadir, Z. Shah, Recent Advances in TiO2-Based Photocatalysts for Efficient Water Splitting to Hydrogen, *Nanomaterials 2025, Vol. 15, Page 984*. **15** (2025) 984. https://doi.org/10.3390/NANO15130984.

[7] H. Ahmad, S.K. Kamarudin, L.J. Minggu, M. Kassim, Hydrogen from photo-catalytic water splitting process: A review, *Renewable and Sustainable Energy Reviews*. **43** (2015) 599–610. https://doi.org/10.1016/J.RSER.2014.10.101.

[8] M. El ouardi, A. El Idrissi, M. Arab, M. Zbair, H. Haspel, M. Saadi, H. Ait Ahsaine, Review of photoelectrochemical water splitting: From quantitative approaches to effect of sacrificial agents, oxygen vacancies, thermal and magnetic field on (photo)electrolysis, *International Journal of Hydrogen Energy*. **51** (2024) 1044–1067. https://doi.org/10.1016/J.IJHYDENE.2023.09.111.

[9] M. Hillenbrand, C. Helbig, R. Marschall, Supply risk considerations for photoelectrochemical water splitting materials, *Energy & Environmental Science*. **17** (2024) 2369–2380. https://doi.org/10.1039/D3EE04369J.

[10] C. Cheng, W. Zhang, X. Chen, S. Peng, Y. Li, Strategies for improving photoelectrochemical water splitting performance of Si-based electrodes, *Energy Science and Engineering*. **10** (2022) 1526–1543. https://doi.org/10.1002/ese3.1087.

[11] C. Ros, T. Andreu, J.R. Morante, Photoelectrochemical water splitting: a road from stable metal oxides to protected thin film solar cells, *Journal of Materials Chemistry A*. **8** (2020) 10625–10669. https://doi.org/10.1039/D0TA02755C.

[12] A.-G. Olabi, A.S. Aricò, A. Pettinau, A. Jilani, H. Ibrahim,

Development in Photoelectrochemical Water Splitting Using Carbon-Based Materials: A Path to Sustainable Hydrogen Production, *Energies 2025, Vol. 18, Page 1603*. **18** (2025) 1603. https://doi.org/10.3390/EN18071603.

[13] A. Ziti, B. Hartiti, H. Labrim, S. Fadili, A. Batan, A. Ridah, P. Thevenin, Growth and Characterization of CZTS Thin Films Synthetized by Electrodeposition Method for Photovoltaic Applications, *IOP Conference Series: Materials Science and Engineering*. **948** (2020) 012025. https://doi.org/10.1088/1757-899X/948/1/012025.

[14] K.Ç. Demir, The investigation of the corrosion behavior of CZTS thin films prepared via electrodeposition, *Materials Science in Semiconductor Processing*. **123** (2021). https://doi.org/10.1016/j.mssp.2020.105553.

[15] Y. Zhang, S. Zhou, K. Sun, Cu2ZnSnS4 (CZTS) for Photoelectrochemical CO2 Reduction: Efficiency, Selectivity, and Stability, *Nanomaterials*. **13** (2023). https://doi.org/10.3390/NANO13202762,.

[16] Y.H. Zhai, Y.X. Peng, Y. Hong, Y.M. Chen, G.Y. Zhou, W. He, P.J. Wang, X.M. Chen, C. Wang, Synthesis and Evaluation of Organic Additives for Copper Electroplating of Interconnects, *Journal of Electrochemistry*. **29** (2023). https://doi.org/10.13208/J.ELECTROCHEM.2208111.

[17] J. Wei, M. Zhou, A. Long, Y. Xue, H. Liao, C. Wei, Z.J. Xu, Heterostructured Electrocatalysts for Hydrogen Evolution Reaction Under Alkaline Conditions, *Nano-Micro Letters*. **10** (2018). https://doi.org/10.1007/S40820-018-0229-X,.

[18] X. Xu, Z. Hao, J. Wang, X. Chen, J. He, J. Cui, K. Yan, J. Li, T. Wang, C. Ren, H. Liu, Electrodepositing high-quality gold coatings in sulfite electrolyte: Experimental and theoretical study on the synergistic behavior of thiomalic acid and HEDP, *Applied Surface Science*. **688** (2025) 162370. https://doi.org/10.1016/J.APSUSC.2025.162370.

[19] J. Ge, Y. Yan, Controllable Multinary Alloy Electrodeposition for Thin-Film Solar Cell Fabrication: A Case Study of Kesterite Cu2ZnSnS4, *IScience*. **1** (2018) 55–71. https://doi.org/10.1016/J.ISCI.2018.02.002.

[20] M.G.C. Beh, B. Hartiti, A. Ziti, F.K. Konan, A. Batan, H. Labrim, A. Laazizi, C.T. Haba, P. Thevenin, Optical and structural properties of CZTS thin films produced by electrodeposition, *Materials Today: Proceedings*. (2024). https://doi.org/10.1016/j.matpr.2024.03.029.

[21] R.R. Widakusuma, Fathir Azzaki Iradata, Mokhamad Ali Rizqi Maulana, Ikhwan Nur Rahman, Electrodeposition of Thin Film Cu-Zn-Sn Alloy for Water Splitting Application, *Chemistry and Materials*. **3** (2024) 81–90. https://doi.org/10.56425/cma.v3i3.82.

[22] E. Peksu, H. Karaagac, Preparation of CZTS thin films for the fabrication of ZnO nanorods based superstrate solar cells, *Journal of Alloys and Compounds*. **884** (2021) 161124. https://doi.org/10.1016/J.JALLCOM.2021.161124.

[23] A.M. Badkoobehhezaveh, H. Abdizadeh, M.R. Golobostanfard, Electrophoretic behavior of solvothermal synthesized anion replaced Cu2ZnSn(SxSe1-x)4 films for photoelectrochemical water splitting, *International Journal of Hydrogen Energy*. **43** (2018) 11990–12001. https://doi.org/10.1016/J.IJHYDENE.2018.04.140.

[24] H. Borate, A. Bhorde, B. Gabhale, S. Pandharkar, M. Prasad, V. Sharma, A. Rokade, S. Jadkar, Single-step Electrodeposition of Cu2ZnSnS4 (CZTS) Thin Film: Influence of Complexing Agent Concentration, *ES Materials and Manufacturing*. **17** (2022) 34–43. https://doi.org/10.30919/ESMM5F723.

[25] T.A. Atesin, S. Bashir, J.L. Liu, Nanostructured materials for next-generation energy storage and conversion: Photovoltaic and solar energy, *Nanostructured Materials for Next-Generation Energy Storage and Conversion: Photovoltaic and Solar Energy*. (2019) 1–501. https://doi.org/10.1007/978-3-662-59594-7.

[26] J. Su, Y. Wei, L. Vayssieres, Stability and Performance of Sulfide-, Nitride-, and Phosphide-Based Electrodes for Photocatalytic Solar Water Splitting, *Journal of Physical Chemistry Letters*. **8** (2017) 5228–5238. https://doi.org/10.1021/ACS.JPCLETT.7B00772,.

[27] E.S. Cama, M. Pasini, U. Giovanella, F. Galeotti, Crack-Templated Patterns in Thin Films: Fabrication Techniques, Characterization, and Emerging Applications, *Coatings 2025, Vol. 15, Page 189*. **15** (2025) 189. https://doi.org/10.3390/COATINGS15020189.

[28] P. McArdle, A. Erxleben, Crystal growth and morphology control of needle-shaped organic crystals, *CrystEngComm*. **26** (2024) 416–430. https://doi.org/10.1039/D3CE01041D.

[29] R.B. Mahewar, L.S.R. lowast, Structure, morphology and optical parameters of spray deposited CZTS thin films for solar cell applications, *Indian Journal of Science and Technology*. **13** (2020) 2149–2156. https://doi.org/10.17485/IJST/V13I21.642.

[30] J.P.S. Mota, V.F. Nunes, F.M. Lima, P.H.F.M. Júnior, W.N. da Silva, C.F. de Andrade, A.S.B. Sombra, A.F.L. Almeida, F.N.A. Freire, Synthesis and characterization of CZTS films, *Matéria (Rio de Janeiro)*. **30** (2025) e20250099. https://doi.org/10.1590/1517-7076-RMAT-2025-0099.

[31] K. Sun, F. Liu, X. Hao, K. Sun, F. Liu, X. Hao, Kesterite $Cu_2ZnSnS_{4-x}Se_x$ Thin Film Solar Cells, *Thin Films Photovoltaics*. (2021).

https://doi.org/10.5772/INTECHOPEN.101744.

[32] M.Z. Ansari, S. Singh, N. Khare, Visible light active CZTS sensitized CdS/TiO2 tandem photoanode for highly efficient photoelectrochemical hydrogen generation, *Solar Energy*. **181** (2019) 37–42. https://doi.org/10.1016/J.SOLENER.2019.01.067.

[33] B. Unveroglu, G. Zangari, Photoelectrochemical Behavior of Bismuth-Containing Cu 2 ZnSnS 4 (CZTS) Absorber Layers for Photovoltaic Applications , *Journal of The Electrochemical Society*. **166** (2019) H3040–H3046. https://doi.org/10.1149/2.0081905JES/XML.

[34] M.P. Suryawanshi, S.W. Shin, U. V. Ghorpade, K. V. Gurav, G.L. Agawane, C.W. Hong, J.H. Yun, P.S. Patil, J.H. Kim, A. V. Moholkar, A chemical approach for synthesis of photoelectrochemically active Cu2ZnSnS4 (CZTS) thin films, *Solar Energy*. **110** (2014) 221–230. https://doi.org/10.1016/J.SOLENER.2014.09.008.

[35] M. Ali, E. Pervaiz, T. Noor, O. Rabi, R. Zahra, M. Yang, Recent advancements in MOF-based catalysts for applications in electrochemical and photoelectrochemical water splitting: A review, *International Journal of Energy Research*. **45** (2021). https://doi.org/10.1002/er.5807.

[36] F. Sun, S. Zhu, Z. Liu, C. Liu, K. Jiang, Y. Zhang, B. Chen, S. Zheng, Data-driven design of metal oxide electrocatalysts with low tafel slope in oxygen evolution reaction, *Journal of Alloys and Compounds*. **1031** (2025) 180964. https://doi.org/10.1016/J.JALLCOM.2025.180964.

[37] B. V. Jegdic, B.M. Radojković, B.M. Bobić, M.M. Krmar, S. Ristić, Corrosion resistance of metalized layers on steel parts in ventilation mill, *Metallurgical & Materials Engineering*. **24** (2018) 123–132. https://doi.org/10.30544/340.

[38] S. Hastuty, H.A. Prasetyo, N.N. Kirana, A. Nugroho, H.S. Oktaviano, M. Awwaluddin, The Effectivity of Oil Palm Inhibitor Processed by Aminolysis to Control Corrosion on Steel in Sodium Chloride Environment, *Journal of Physics: Conference Series*. **2080** (2021) 012027. https://doi.org/10.1088/1742-6596/2080/1/012027.